IOP Publishing Journal of Micromechanics and Microengineering

J. Micromech. Microeng. **17** (2007) S224–S229 doi:10.1088/0960-1317/17/9/S03

Encapsulated ball bearings for rotary micro machines

C Mike Waits[1,2], Bruce Geil[2] and Reza Ghodssi[1]

[1] MEMS Sensors and Actuators Laboratory (MSAL), Department of Electrical and Computer Engineering, Institute for Systems Research, College Park, MD 20742, USA
[2] US Army Research Laboratory, 2800 Powder Mill Road, Adelphi, MD 20783, USA

E-mail: ghodssi@umd.edu

Received 26 February 2007, in final form 8 August 2007
Published 31 August 2007
Online at stacks.iop.org/JMM/17/S224

Abstract

We report on the first encapsulated rotary ball bearing mechanism using silicon microfabrication and stainless steel balls. The method of capturing stainless steel balls within a silicon race to support a silicon rotor both axially and radially is developed for rotary micro machines and MEMS ball bearing tribology studies. Initial demonstrations show speeds up to 6.8 krpm without lubrication, while speeds up to 15.6 krpm with lubrication are possible. Qualitative analysis is used to explain start-up behavior and investigate the wear of the stainless steel ball and silicon race.

(Some figures in this article are in colour only in the electronic version)

1. Introduction

Micro electromechanical systems (MEMS) fabricated silicon rotary elements for micro-motors, micro-generators and micro-turbomachinery have received growing attention with applications in power conversion and actuation. Within these technologies, the bearing mechanism is the primary determinant of device performance and reliability. Both active and passive bearings have been investigated for rotary motion; however, no known successful commercial implementations are known due to poor reliability and short lifetimes. Active bearings, such as magnetic or electrostatic have the advantage of being controlled during the operation, but at the cost of the accompanying circuitry [1]. Passive bearings have been investigated heavily and span a large range of velocities that include center-pin bushings with low revolution rates possible [2, 3] and hydrostatic or hydrodynamic bearings with high revolution rates possible [4]. Contact passive bearing mechanisms have poor reliability characteristics and are limited to low speeds due to the high frictional forces of sliding motion [2]. In contrast, non-contact bearings based on active elements, or pressurized gas, have been demonstrated to achieve high speeds but require complex fabrication procedures with tight tolerances [3].

Tan *et al* [5] have investigated the tribology of a linear ball bearing mechanism and showed that the frictional properties between 440C stainless steel balls and silicon are quite low when compared to pure sliding motion due to the rolling nature. The frictional properties of ball bearings allow the possibility for higher speeds and better reliability than other contact bearings relying on sliding motion while maintaining fabrication simplicity and stability. Although ball bearings have been demonstrated in devices such as linear micromotors [6, 7] and rotary micromotors [8], they have yet to be integrated into the microfabrication process to fully constrain the dynamic element. In the cases of both Modafe *et al* [6] and Ghalichechian *et al* [7, 8] the dynamic element, whether it is a rotor or a linear slider, is held onto the balls by an electrostatic force. Their approach requires an additional force to maintain contact between the dynamic element and the stator. This imposes restrictions in the manufacturing process and assembly with the surrounding system components. Furthermore, a testing platform capable of investigating speeds greater than 100's rpm for ball bearings has yet to be developed.

Hence, a rotary ball bearing mechanism is reported here wherein the rolling elements are encapsulated at the periphery of the rotor to enable high speed rotation without relying on any attractive force between the rotor and stator. An experimental test stand is implemented to demonstrate the encapsulated bearing operation at rotational speeds up to 16 krpm and serve as a stepping-stone for future high speed and high load tribology experiments. Results for both dry and lubricated, full compliment bearings are also reported leading toward the development of micro turbomachinery. A qualitative analysis is given for the wear seen on the silicon race and the

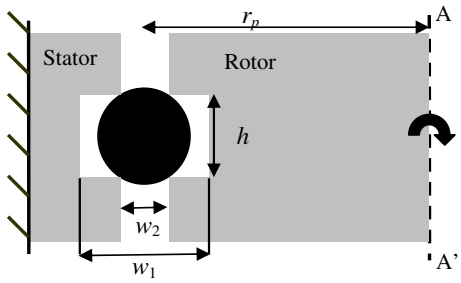

Figure 1. Schematic drawing showing the design of the ball bearing mechanism. The rotational axis of the rotor is shown by the A–A′ dashed line on the right-hand side of the drawing.

Table 1. Dimensions of the ball bearing mechanism.

Parameter	Dimension
d_{ball}	285 μm
r_{p}	4 mm
$h = d_{\text{ball}}/\sqrt{2}+ \delta h$	205 μm
w_1	300 μm
$w_2 = d_{\text{ball}}/\sqrt{2}+ \delta w_2$	205 μm

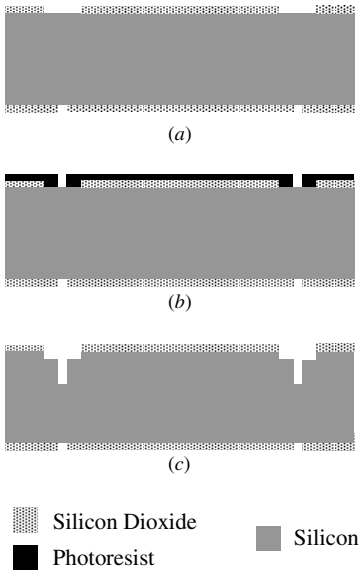

Figure 2. Simplified fabrication flow for the silicon race using a nested masking layer and two DRIE steps.

stainless steel ball and correlated to the start-up behavior of the bearings.

2. Race design

The design and fabrication of the rotary ball bearing is based on commercially available 440C stainless steel balls with a diameter, d_{ball}, of 285 μm and a lot diameter variation of 0.254 μm (see figure 1). The design features balls housed at the periphery of the rotor to enable a two-layer fabrication sequence for encapsulation via bonding. At the same time, this scheme of encapsulation allows features to be patterned on either side of the rotor while having minimal influence from the bearings.

A square groove race was designed to encase the micro ball bearings. Alternative designs, nevertheless, may be able to improve the performance and fatigue characteristics of the bearings. One can easily think of methods to incorporate race designs which better mimic those from their macroscopic counterparts, such as a rounded groove race or an angular contact race; however, these may require more stringent fabrication processes. Housing the balls using a square groove race fabricated by a dry anisotropic etch process, such as deep reactive ion etching (DRIE), allows control of the contact points and better repeatability when compared to other race designs and fabrication methods.

The dimensions of the ball bearing mechanism are listed in table 1. The ball race was designed to have a pitch radius, r_{p}, of 4 mm from the rotational axis to the center of the race. The width of the outer ring, w_1, is 300 μm to ensure the balls fit into the race with the fabrication tolerances involved. The width of the nested race, w_2, is $d_{\text{ball}}/\sqrt{2} + \delta w_2$, so that the balls contact at the 90° corners or 205 μm with the tolerances, δw_2, added in. The total height of the race between the contact points, h, is the same as the width, w_2. Both δh and δw_2 are made 4.5 μm to include fabrication tolerances and thermal expansion differences during bonding. Furthermore, the ratio of h/w_2 can be varied to change the incident angle of the load on the corners of the race where the wear rate of the silicon will be at a maximum.

3. Encapsulated ball bearing fabrication

The bearing mechanism is fabricated in three major steps: (1) silicon races are fabricated on the wafer level; (2) balls are placed into the race and an identical race is bonded on top to encapsulate them; and (3) silicon DRIE is used to release the rotor.

The steps used to fabricate the silicon races are illustrated in figure 2. A double-sided polished, (1 0 0) silicon wafer with a thickness of 440 μm was used with a 1.1 μm silicon dioxide layer thermally grown on the surfaces. The silicon dioxide on the top-side of the wafer was patterned with the outer ring of width w_1 and a pitch radius of 4 mm. The silicon dioxide on the bottom-side of the wafer was patterned with a ring of width w_2. Figure 2(*a*) shows these steps with both the top and bottom silicon dioxides patterned. A concentric ring of width, w_2, was then aligned and patterned into photoresist on the top-side of the wafer, shown in figure 2(*b*). Together, the patterned photoresist and patterned silicon dioxide form a nested masking layer. Two DRIE steps using a Unaxis VLR 700 system were employed to form the silicon race using the photoresist as the first masking layer and the silicon dioxide as the second masking layer. The result of the nested masking layer etching is illustrated in figure 2(*c*). This forms a silicon race in which two identical dies on a wafer can be bonded together and encapsulate the balls.

A 1.15 μm Cr/Au/AuSn/Au metal adhesion layer is employed to encapsulate the balls and the device is released using DRIE. The metal layers were chosen from in-house device packaging experience as well as its low softening temperature below 300 C to later de-bond for inspection. This process is shown in figure 3. The metal adhesion layer is deposited using electron beam evaporation through a silicon

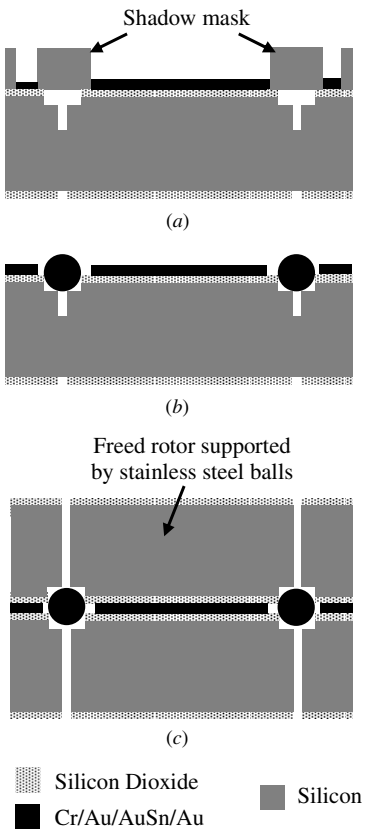

Figure 3. Fabrication flow showing encapsulation using a Cr/Au/AuSn/Au adhesion layer and release using DRIE.

shadow mask, shown in figure 3(*a*). After metal deposition, the wafer is diced into individual die for bonding.

Balls are manually placed into the silicon race of one die, figure 3(*b*), and an identical silicon race is aligned using balls strategically placed into square alignment pits at the corners of the die. The number of the balls placed into the race must be more than necessary to fill half of the silicon race. Above this number, the balls were chosen arbitrarily. The alignment pits are etched into the silicon at the same time as the race and, therefore, are etched to a specified depth in which only half of the ball protrudes out of the pit. By doing so, a 290 μm wide pit and a 285 μm diameter ball will result in a maximum misalignment of 5 μm. The aligned stack is then bonded together using a Karl Suss SB6 wafer bonder with a 1 kTorr applied pressure at a temperature of 285 °C using a 1.33 kTorr H_2N_2 forming gas atmosphere. After bonding, DRIE is used to etch through the silicon using the previously patterned silicon dioxide to release the rotor shown in figure 3(*c*).

Figure 4 shows a photograph of a silicon race die before bonding with the metal adhesion layer deposited. The square pits used for alignment of the die before bonding can be seen in the corners of the die. Figure 5 shows a photograph of a completely released bearing with the silicon dioxide mask remaining. In most cases, the silicon rotor is completely released after the DRIE steps; however, in some cases metal particles form in the bearing race due to reflow of the metal adhesion layer during the bonding process. After the final release some of the particles are too large to be removed from

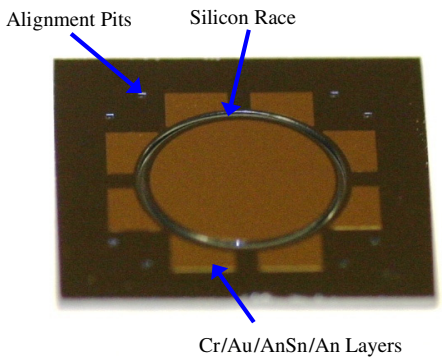

Figure 4. Optical picture of a die showing the patterned race, metal and alignment pits.

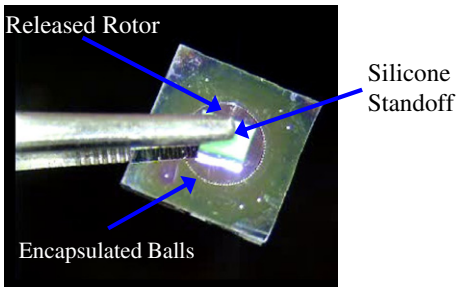

Figure 5. Optical picture of a released silicon rotor supported by stainless steel balls at the periphery. A full compliment configuration was used with more than 60 balls.

the race preventing the rotor from spinning thereby lowering fabrication yield.

Other bonding techniques such as silicon fusion bonding are better suited when fabricating final devices for use in actual systems; however, they typically produce permanent bonds which are not conducive for investigating purposes. To investigate the silicon race and stainless steel balls after operation a temporary bonding method is better suited. Metal adhesion allows the bearing mechanism to be separated on a hotplate allowing easy inspection.

4. Experimental setup and results

Demonstration of the encapsulated ball bearing was accomplished using the setup shown in figure 6. Standoffs are placed on both the top and bottom of the rotor and the stack is held in place using a mechanical vice. A nitrogen line is placed within 2 mm of the die corner using a second mechanical vice. The flow from the nitrogen line causes the outer portion of the die to spin about the clamped center. A Philtec D6 Fiberoptic displacement sensor is used to measure the angular velocity of the spinning square die.

Initial movement of the square die about the center required a line pressure greater than 5 psi for most of the devices tested. Lower pressures were not able to produce enough force on the edge of this square die to counteract static friction, which is much higher than the dynamic friction once it is rotating. In some cases, bearings have to be manually started to overcome this initial friction. Once they are spinning, line pressures as low as 1 psi have been used to maintain operation.

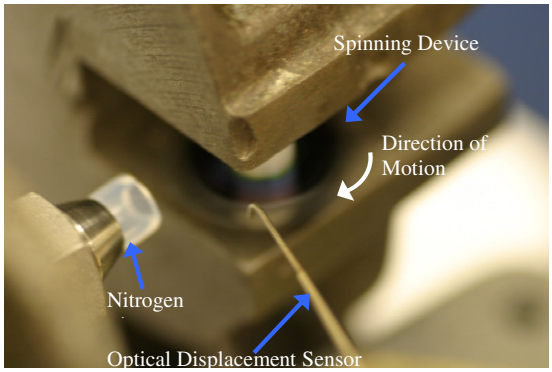

Figure 6. Optical picture of the test set-up used to measure the speed of the rotating bearing mechanism.

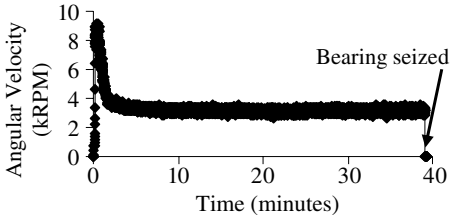

Figure 7. Angular velocity versus time showing the initial start-up transient and settle speed for a constant l5.5 psi line pressure.

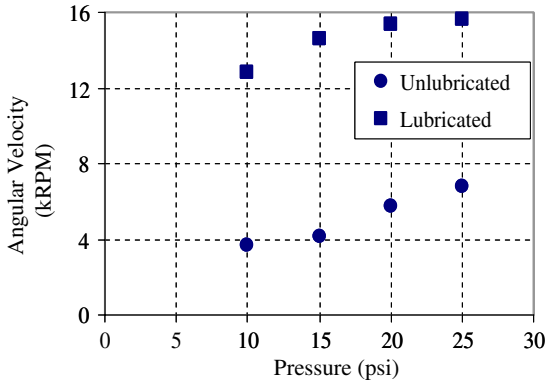

Figure 8. Measured speed of a bearing versus nitrogen line pressure with and without JP-8 lubrication.

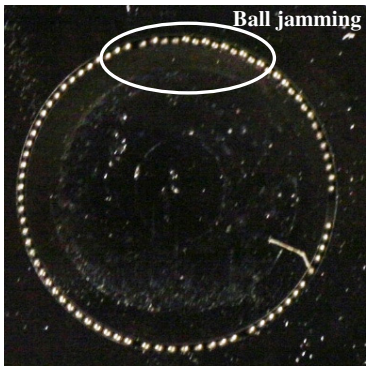

Figure 9. Optical picture of ball jamming occurring within the ball bearing race.

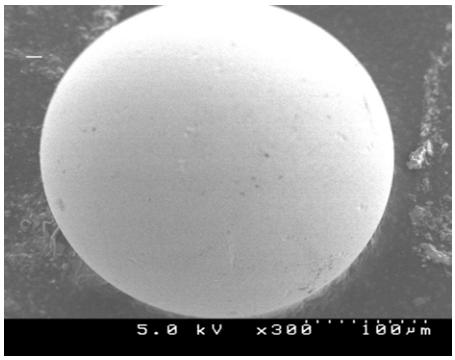

(*a*)

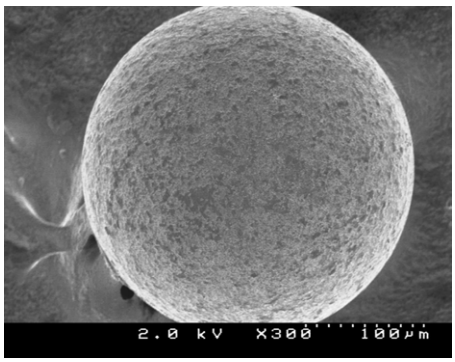

(*b*)

Figure 10. SEM images showing (*a*) fresh stainless steel ball and (*b*) stainless steel after 39 min of an average 3.2 krpm rotation rate.

Figure 7 shows the angular velocity versus time using a nitrogen line pressure of 5.5 psi and a device which had 70 stainless steel balls. A start-up transient is clearly seen in which the device rotates at a rate greater than 9 krpm, but then drops to an average rate of 3.2 krpm.

Figure 8 shows the results of angular velocity versus an increasing nitrogen line pressure for two cases: (1) dry bearings and (2) lubricated bearings with 82 balls. Such a demonstration shows the potential velocity benefit by only adding lubrication to increase the speed of the device. The pressure was started at 10 psi and increased by 5 psi after each measurement over a period of 12 min. The maximum open pressure of the nitrogen line used was 25 psi. Ball jamming occurred after 12 min of operation causing the device to seize. Figure 9 is an optical picture of a bearing which was stopped due to ball jamming. Slight agitation was used to release the balls allowing the device to spin freely until the race wear became too large where jamming occurred before spinning.

The same device was restarted with 50 μL of JP-8 diesel fuel added into the bearing opening. JP-8 is readily available and has a lubricity additive making it a good lubricant [9]. The device was turned manually to allow uniform coating around the silicon race and over the stainless steel balls. Again the pressure was increased from 10 psi to 25 psi and measurements taken at 5 psi increments over a period of 10 min. The JP-8 evaporated soon thereafter and the bearing seized again due to ball jamming. An increase of 8–9 krpm can be seen between the dry condition and the lubricated condition for each pressure setting.

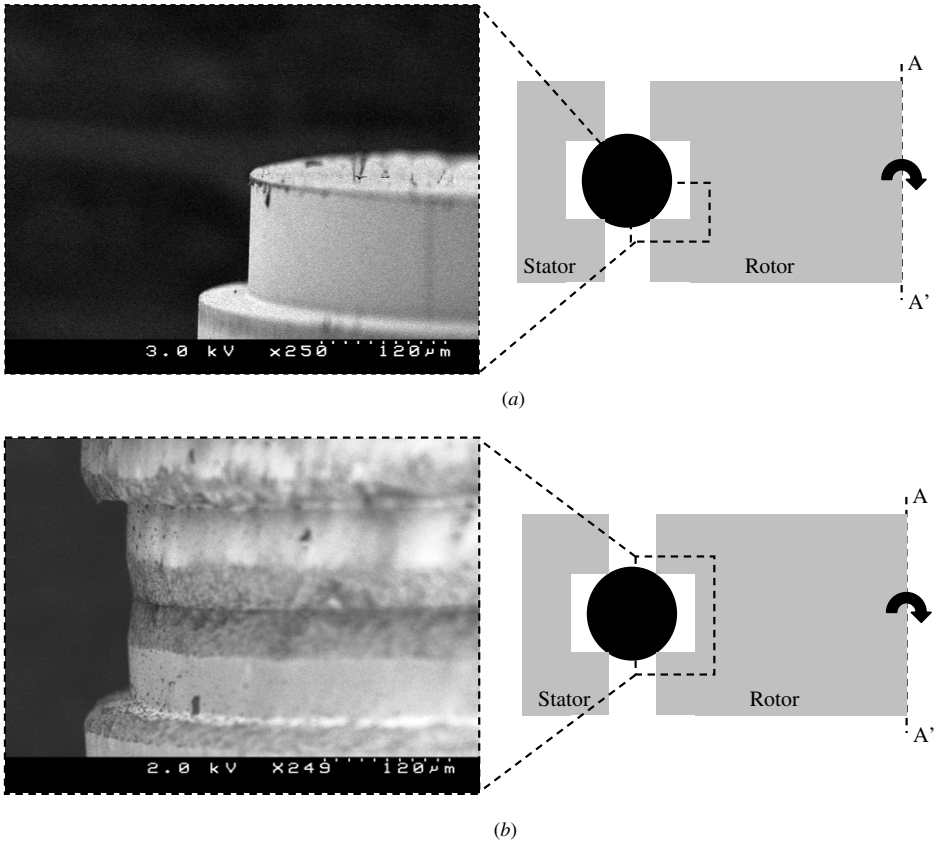

Figure 11. SEM image of a silicon race (*a*) before and (*b*) after testing and a schematic drawing illustrating where the SEM image was taken.

5. Discussion

The testing method employed induces a high load onto the bearing device. This as well as the square groove race design and the brittle silicon material lead to high wear. Scanning electron microscopy (SEM) images were used to investigate the wear of the silicon race and of the stainless steel balls. The device which operated for 39 min in figure 7 before jamming was separated on a hot plate at 400 °C. Figures 10 and 11 are SEM images showing the wear of the stainless steel ball and the silicon race, respectively.

The start-up behavior exhibited in figure 7 is believed to arise from wearing of the race and ball. As the surfaces roughen more friction is assumed to occur, slowing the angular velocity of the device for a constant applied force. The wear rate is a function of the maximum stress incurred on the silicon race by the loaded ball. The maximum stress occurs at the central point of the contact area and can be estimated as [10]

$$\sigma_{\max} = \frac{3Q}{2\pi ab} \tag{1}$$

in which Q denotes the load exerted normal to the race from the ball, a is the semi-major axis radius of an elliptical contact area, and b is the semi-minor axis radius for an elliptical contact. As the silicon race and the ball wear away, both the load and the contact area change. The load changes due to the contact angle, which in this case did not vary significantly. For the wear exhibited in figure 10, the contact area changes from a sharp semi-infinite point to a large flat area. This in turn significantly reduces the compressive stress and decreases the wear rate by orders of magnitude. In the case of figure 7, after the initial 3 min, the compressive stress became low enough for the wear rate to shrink below levels noticeable during short runs; therefore, a relatively constant angular velocity is seen for the remaining 39 min.

Ball jamming which has occurred for both bearing devices reported here is an inherent problem when full compliment type bearings are used. The race dimensions increase as wear ensues giving the balls more play and a greater chance to seize. Implementation of a low wear material on top of the silicon race along with tighter fabrication tolerances can reduce the probability of jamming, but not eliminate it completely. Instead, a retainer ring (or cage) could be used to isolate the balls from one another. In addition to eliminating ball jamming, the use of a retainer ring can greatly reduce the friction since a much smaller number of balls can be used. A retainer ring maintains a separation distance between the balls allowing for a minimum number of balls to be used. Reduction in the friction by decreasing the number of balls will similarly lead to much higher speeds as well as better reliability.

The current method of testing, that is, blowing nitrogen on the face of the bearing die causes a torque about the longitudinal axis. This unwanted torque arises due to a non-uniform nitrogen flow across the top and bottom of the device as well as asymmetric loads on the spinning edge. Additionally, the device is asymmetrically loaded parallel to the nitrogen flow causing more wear on the sides opposing the flow and less on the sides facing away from the flow. Both the undesired torque and the non-uniform loading could

contribute to ball jamming. An improved testing method is being developed to eliminate this effect and greatly increase the operation time of the bearing before jamming occurs.

There are a number of contributing factors leading to increased ball jamming occurrence as well as the overall tribological properties of the bearing mechanism. Firstly, the number of stainless steel balls influences not only the load distribution affecting the induced stress shown in equation (1), but will also affect the amount of friction from surface indentation and ball-to-ball collisions. Secondly, the geometry of the silicon race also has a large influence on the loading and the wear that will occur. More sophisticated race geometries, such as rounded or angular races, will have a big impact into the tribological properties as well as the ball jamming issue. Thirdly, the choice of the ball size and material along with the choice of wet or dry lubrication such as a SiC or diamond deposited film on the silicon race will greatly influence the frictional properties and the factors leading to increased ball jamming. All of these factors should be the focus of future studies to develop a robust and reliable ball bearing mechanism.

6. Conclusions

We have demonstrated the first encapsulated rotary ball bearing platform using silicon microfabrication processes. The platform developed is a step toward more quantitative investigations on the tribological characteristics for the silicon race design reported here, as well as other race/ball designs and materials for MEMS ball bearing mechanisms. The implementation of an encapsulated rotary ball bearing will lead to the development of micro turbomachinery for Power MEMS as well as other microsystem applications.

Acknowledgments

The authors thank the Army Research Laboratory cleanroom personnel for their support in the fabrication of the devices as well as the members of the MEMS Sensors and Actuators Laboratory at the University of Maryland.

References

[1] Coombs T A, Samad I, Ruiz-Alonso D and Tadinada K 2005 *IEEE Trans. Appl. Supercond.* **15** 2312–5
[2] Mehregany M, Gabriel K J and Trimmer W S N 1988 *IEEE Trans. Electron Devices* **35** 719–24
[3] Fan L-S *et al* 1988 *IEEE Trans. Electron Devices* **35** 724–30
[4] Fréchette L G *et al* 2001 *Proc. 14th Annual IEEE Int. Conf. MEMS* pp 290–3
[5] Tan X, Modafe A and Ghodssi R 2006 *J. Dyn. Syst. Meas. Control* **128** 891–8
[6] Modafe A, Ghalichechian N, Frey A, Lang J H and Ghodssi R 2006 *J. Micromech. Microeng.* **16** S182–91
[7] Ghalichechian N, Modafe A, Lang J H and Ghodssi R 2006 *Sensors Actuators A* **136** 416–503
[8] Ghalichechian N, Modafe A, Beyaz M I, Waits C M and Ghodssi R 2006 *6th Int. Workshop on Micro and Nanotechnology for Power Generation and Energy Conversion Applications (Power MEMS '06)* pp 227–30
[9] Edwards T 2007 *J. Eng. Gas Turbines Power* **129** 13–20
[10] Harris T 1991 *Rolling Bearing Analysis* 3rd edn (New York: Wiley) p 158